Refractometer based on phase measuring deflectometry using smartphone and machine learning assisted analysis

Sharma, Shivam; Trivedi, Vismay; Utadiya, Subhash; Sheoran, Gyanendra; Anand, Arun

DOI
10.1088/1402-4896/ae11d7

Publication date
2025

Document Version
Final published version

Published in
Physica Scripta

PAPER • **OPEN ACCESS**

Refractometer based on phase measuring deflectometry using smartphone and machine learning assisted analysis

To cite this article: Shivam Sharma *et al* 2025 *Phys. Scr.* **100** 105540

Physica Scripta

OPEN ACCESS

RECEIVED
27 June 2025

REVISED
23 August 2025

ACCEPTED FOR PUBLICATION
10 October 2025

PUBLISHED
24 October 2025

PAPER

Refractometer based on phase measuring deflectometry using smartphone and machine learning assisted analysis

Shivam Sharma[1,5], **Vismay Trivedi**[1,2,5,*], **Subhash Utadiya**[3], **Gyanendra Sheoran**[1] and **Arun Anand**[4]

[1] Advanced Research in Optical and Microwave Applications (AROMA) Lab, Department of Applied Sciences, National Institute of Technology (NIT), Delhi 110036, India
[2] Department of Aerospace Structures and Materials, Delft University of Technology, Kluyverweg 1, 2629 HS, Delft, The Netherlands
[3] Applied Physics Department, Faculty of Technology and Engineering, The M S University of Baroda, Vadodara, India
[4] Department of Physics, Sardar Patel University, Vallabh Vidyanagar, Anand-388120, India
[5] Contributed equally.
[*] Author to whom any correspondence should be addressed.

E-mail: vismay.trivedi@gmail.com

Keywords: refractive index measurement, phase measuring deflectometry, machine learning, fourier fringe analysis

Supplementary material for this article is available online

Abstract

Measuring refractive index values in transparent liquids has broad applications across industrial, scientific, and technological domains for their identification and characterization. Here a phase measuring deflectometry technique with an artificial fringe system is demonstrated to measure the refractive indices of transparent liquids. It works by projecting a line pattern displayed on a smartphone screen through a test chamber with a unique geometry containing the test solution, which a smartphone camera records. The technique detects changes in refractive index by analyzing phase changes resulting from fringe shifts due to the test solution. The phase difference is determined using Fourier transform-based fringe analysis, and the refractive index is measured by extracting features from the computed phase difference profile and training a regression machine learning algorithm. The developed system is compact, simple, low-cost and accurate. It can measure refractive index with a root mean squared error (RMSE) of 8.5375×10^{-4}, a mean absolute error (MAE) of 7.9×10^{-4}, and a precision of 3.175×10^{-4}.

1. Introduction

The interaction of electromagnetic radiation with a medium can provide valuable insights into the material's properties. The property responsible for slowing the speed of light as it moves through the medium is termed the refractive index (RI), and is expressed as the ratio of the velocity of light in a vacuum to the velocity of light in the observed medium [1, 2]. Monitoring RI is of significant interest across various industrial, scientific, and technological fields due to its role as an optical parameter reflecting material properties. Accurate measurement of the concentration of a solution by computing RI is required in fields including physics, chemistry, and biology [3].

Moreover, Sugar content is a key parameter in assessing harvest maturity, which directly influences shelf life and final product quality [4–6]. Beyond these applications, RI measurement is pivotal in agriculture, wine-making, brewing, material processing and characterization, pharmaceuticals, communication systems, fiber optics, thick and thin films, petrochemical industries, cosmetics, geological surveys, etc [7–16]. In the medical industry, RI measurement is critical in computing the specific gravity of human urine to assess kidney function [17]. Consequently, RI measurement emerges as a necessity across diverse domains, from biological to industrial applications [8], necessitating the development of advanced techniques to address these multifaceted requirements.

Various refractometry techniques have been developed using principles of geometrical and wave optics. Classical methods, such as Abbe's refractometer, determine RI based on the angle of minimum deviation

through a liquid-filled prism [9, 18–21]. More recent approaches utilize optical fibres and rely on total internal reflection (TIR), evanescent waves, fibre Bragg gratings (FBG), surface plasmon resonance (SPR), and photonic crystal [22–26]. While these methods offer high sensitivity, they often require complex and expensive optical components for sensor design and calibration [11]. Laser speckle-based RI measurement has also been reported because of its simplistic design and high sensitivity [27, 28]. The simplistic design had allowed the measurement system to take the shape of a portable, hand-held, and sturdy device [27–29]. Although these approaches provide high resolution, they depend on the bulk behaviour of the material, and the localized value of RI cannot be determined. Digital holography enables localized RI mapping [13, 30–32] but suffers from limited dynamic range and sensitivity to vibrations.

One technique that can meet the conditions of simplistic design, compact form factor, flexibility in measurement sensitivity and range, and affordability is phase measuring deflectometry (PMD). In the case of PMD, a screen displaying a fringe pattern is either imaged through the object (for a transparent object) or upon specular reflection from a shiny surface [33–37]. Because of the optical thickness (refractive index multiplied by the actual thickness) of the object present in between the screen and recording device, the light experiences refraction, due to which the recorded fringe pattern gets modulated (shifted). In the transmission geometry used in this study, sinusoidal fringe patterns are imaged through a transparent sample, and their distortion due to refractive index gradients is captured using a camera. These fringe shifts are analysed using fringe analysis to extract the phase gradient, which is related to the optical path variation. This modulation in the fringe pattern is digitally recorded and then numerically processed using fringe analysis algorithms to obtain phase information (proportional to the angle of bending/deflection) related to the optical thickness gradient [38, 39]. Samples exhibiting distinct refractive indices kept in an experimental chamber will result in different optical thickness gradients, leading to different modulations in the projected fringe pattern. This could be leveraged for the measurement of the refractive index of test samples. The versatility of PMD in transmission mode has also been demonstrated in our recent study on phase contrast microscopy, where local fringe deflections were used to visualize transparent microstructures and quantify their thickness [40]. It has also been applied to visualize heat flow and detect thermal anomalies in metallic materials, where heat-induced refractive index gradients in a transparent medium distorted fringe patterns, enabling compact, emissivity-independent, and surface-independent thermal diagnostics through PMD [41]. This underlines the adaptability of PMD for quantitative optical metrology. To the best of our knowledge, this is the first implementation of transmission-mode phase measuring deflectometry for refractive index quantification that leverages a dual-purpose consumer device and machine learning–based regression.

Recent advancements in machine learning have demonstrated their effectiveness in prediction and classification tasks [42, 43]. These techniques have been combined with optical methods such as fiber interferometers [44, 45], colorimetric metasurfaces [46], and laser specklegrams [47] for refractive index (RI) prediction. In this study, we present the development of a simple, low-cost, and robust refractometer for transparent liquids based on phase measuring deflectometry (PMD) employing Fourier fringe analysis to extract phase information. The features obtained from the computed phase maps are used to train regression algorithms [42, 43], generating a machine learning model capable of predicting the refractive index of unknown liquid solutions. The RI measurement system employs a simple design, utilizing a smartphone screen to display fringe patterns and a smartphone camera to capture modulated fringe images, making the system both affordable and user-friendly. The device demonstrated an average prediction error (RMSE) of 8.5375×10^{-4}, reflecting its measurement accuracy and precision of 3.175×10^{-4}, as indicated by the standard deviation of the predicted refractive indices [48, 49]. The mean absolute error (MAE) was also calculated to be 7.9×10^{-4}, providing an additional measure of typical prediction error.

2. Phase measuring deflectometry for refractive index measurement

In the transmission mode, the phenomenon that governs PMD is refraction, wherein the light passing through the object bends or deflects toward regions of higher optical path length [50]. The bending of light rays can be quantified by computing the change in the projected fringe pattern recorded with the object of interest kept between the fringe pattern and the imaging system [35]. The proposed refractometer (figure 1) quantifies the angle of bending or deflection of the light ray, which leads to the shifting (modulation) of the projected fringe pattern. The fringe phase information can be extracted using various fringe analysis techniques [51]. However, due to its simplicity and effectiveness, the Fourier transform-based fringe analysis, which is used in the present technique, is a widely used algorithm in optical metrology, particularly for phase measurement [52, 53]. The bending of the light ray passing through the sample is proportional to the gradient of the optical thickness perpendicular to the direction of fringe orientation. Hence, the Fourier analysis of the recorded fringe system yields the gradient phase and thus needs to be integrated along the length of the object in the direction of the

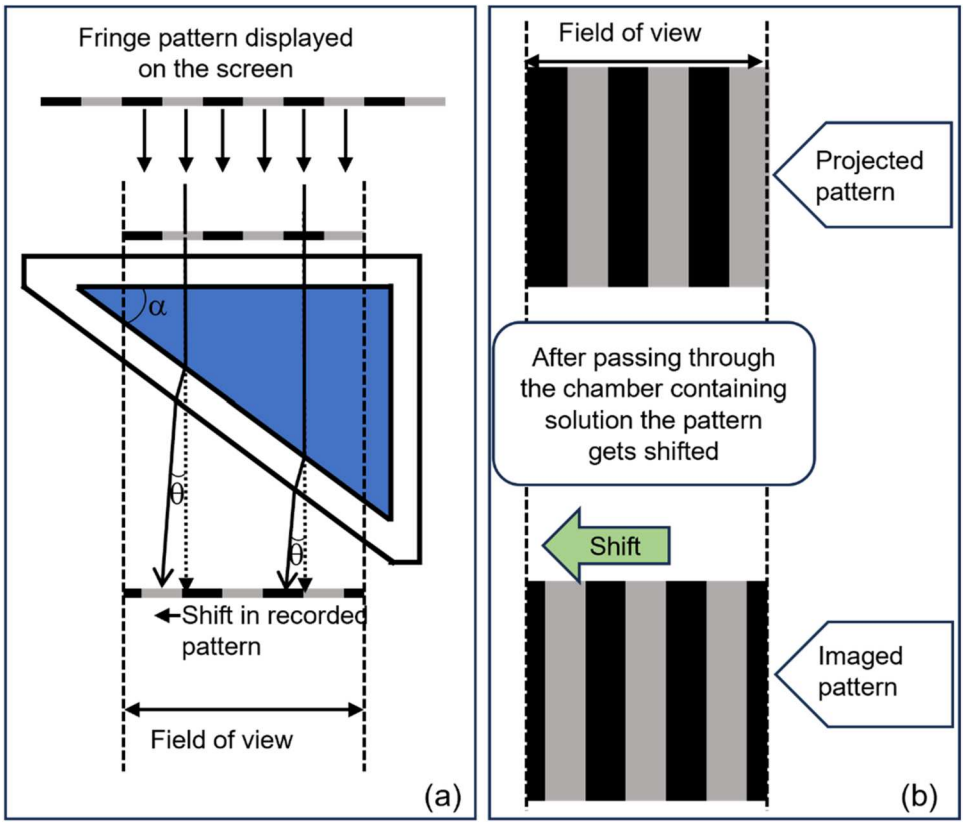

Figure 1. Shift in the fringe pattern projected through the hollow prism filled with test solution.

change in the fringe pattern [54]. This integrated phase profile could be used as a measure of RI of the object in the case of a sample having uniform refractive index.

In this work, a fringe pattern is imaged through a hollow prism (fused silica, thickness ~170 μm, refractive index = 1.52) filled with liquid, the refractive index of which is to be determined. The hollow prism is kept so that one side is aligned parallel to the screen, displaying a fringe pattern. The other side is at an angle ($\alpha = 45°$) with the screen, as shown in the figure 1(a). Due to the introduction of the liquid, the image of the fringe pattern experiences a lateral shift (due to optical thickness variation), as demonstrated in figure 1(b). This lateral shift in the fringe pattern is proportional to the RI of the liquid. Hence, liquids with different RI values produce different lateral shifts. This effect serves as the basis for the proposed RI measurement technique.

In the proposed approach, the image of the fringe pattern recorded through a chamber filled with distilled water serves as the reference. When a transparent phase object (in our case sugar solution) is introduced between the displayed fringe system and the imaging system, due to the change in the optical path length experienced by the light beam while passing through the object, the image of the fringe pattern gets deflected which leads to the modulation of the original fringe pattern. The angle of deflection of the light beam is $\alpha \approx \left(\frac{\partial S(x,y)}{\partial y}\right)$, where $S(x, y)$ is the optical path length accumulated by the light beam passing through the phase object at position (x, y). If d is the distance between the fringe pattern and the object, the fringe shifts in the y direction by distance $\alpha d \approx d\left(\frac{\partial S(x,y)}{\partial y}\right)$ [55]. So, the phase associated with the numerically processed fringe pattern is proportional to the deflection angle α. Thus, it can be inferred that the gradient of optical thickness is proportional to the phase, which in turn is proportional to the deflection angle.

After applying the Fourier fringe analysis to the recorded images which provides the gradient phase associated with both the reference (distilled water: ϕ_W) and each concentration of sugar solutions (ϕ_S). The gradient phase change $\Delta\phi$ ($\phi_S - \phi_W$) due to the shift in the fringe pattern was computed using the Fourier fringe analysis approach, as shown in the flow chart in figure 2. The system measures RI by extracting features based on the computed integrated phase difference profile that was obtained by comparing the phase associated with each RI value with the reference phase that is associated with distilled deionized water. These features were then used to train a linear regression machine learning algorithm to predict/measure the RI values of the liquids under observation. The machine learning algorithm works on the computed phase difference profile extracted by the PMD system and not directly on images. In this work, the input to the machine learning models is not the

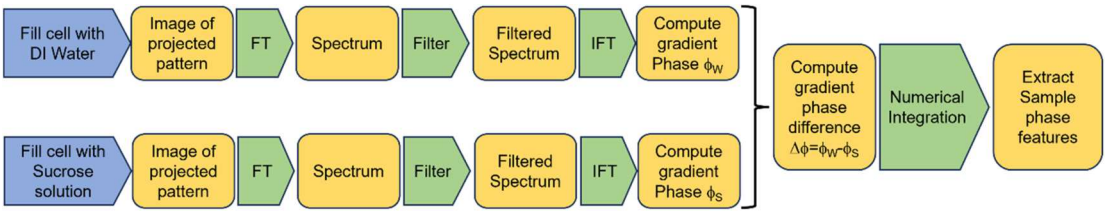

Figure 2. Fringe analysis using Fourier Transform algorithm.

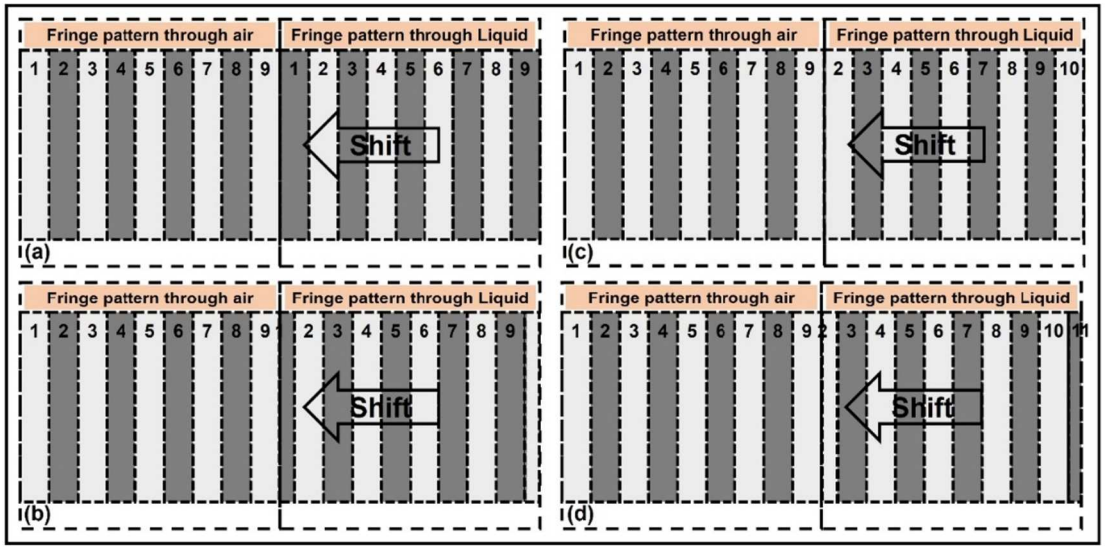

Figure 3. Fringe shift due to increase in refractive index of the solution inside the experimental chamber. (a)–(d) represents an increase in refractive index.

raw image but a set of features extracted from the unwrapped (continuous phase) phase maps, including mean, variance, and gradient-based measures. All algorithms are trained and evaluated on the same train-test feature set, ensuring a consistent basis for comparison. Image-based algorithms (such as CNN) have not been used in the proof-of-concept experiments.

In the present case, the fringe orientation (vertical fringe) is along the direction perpendicular to the change in the optical thickness of the experimental chamber (hollow prism). The recording device records the fringe pattern imaged through the air (outside the chamber) and the liquid, as depicted in figure 3. The fringe pattern projected through the experimental chamber shifts along the direction of the change in the optical thickness. In contrast, the pattern projected through the air remains the same. As the difference between the refractive indices of air (reference—left side of the field of view) and the experimental solution (sucrose in the present case) increases, the shift in the fringe pattern also increases.

Since the sensitivity and the range of the system depend only on the relative shift in the fringe pattern, the system treats cases shown in figures 3(a) and (c) as the same (with opposite phase differences). This means that the value of the computed phase difference after a shift of one fringe in the fringe pattern will be opposite in phase and the same in magnitude. In other words, the phase difference values increase from figures 3(a) to (c), and after (c), the phase difference value gets reversed and repeated, as shown in figures 3(b) and (d). Thus, for a particular fringe density, a shift of one fringe is the maximum change the system can quantify, representing the range of measurable refractive index.

3. Experimental realization

Figure 4(a) shows the schematic of the experimental setup, while figure 4(b) shows the actual experimental setup. The experimental system includes a smartphone screen (display resolution: 720 × 1280 at 267ppi, 408 NITS) to display the fringe pattern (fringe density of $p = 7.3$ line pair per centimeter on the display screen) that is being imaged by a smartphone camera (resolution: 1080p, 0.8 μm pixel pitch). The liquid under observation

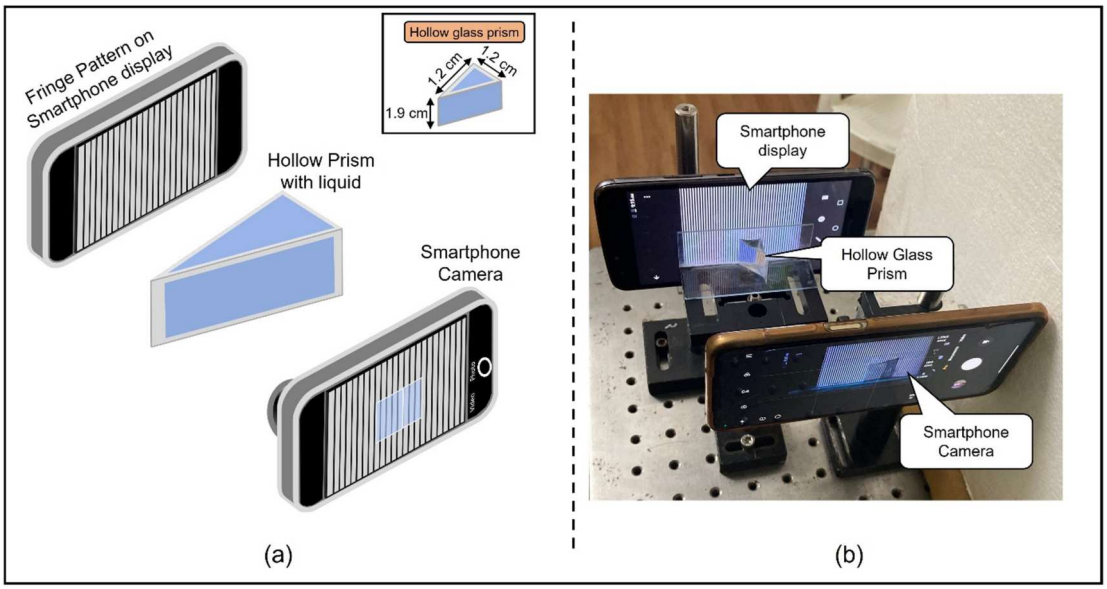

Figure 4. Experimental Setup for measuring refractive index using phase measuring deflectometry.

was kept inside the hollow prism (volume = 1.35 ml, at a distance $d = 1$ cm from the screen), which is placed between the screen and the camera, as shown in figure 4. The base of the hollow prism was parallel to the screen, as shown in figure 4.

Aqueous solutions of sucrose of different concentrations (2.5% w/v to 40% w/v in the step of 2.5% w/v) were prepared to generate 16 different values of refractive indices (1.3355 to 1.3970) [56]. The fringe pattern associated with each RI value is compared with the fringe pattern associated with distilled water (0% w/v) to obtain the change in RI in terms of phase information.

The experimental chamber was filled with the solutions serially, and the vertical fringe pattern described in the previous section was projected through the chamber and imaged. This procedure was repeated ten times. So, a total of 160 projected patterns were recorded. A set of reference fringe patterns was recorded by filling the experimental chamber with distilled deionized water for phase comparison. The central wavelength of the projected light lies at around 610 nm (FWHM = 52 nm). Supplementary figure S1 shows the recorded spectrum of the display device for the projected pattern. Figures 5(a) to (d) shows the recorded fringe patterns for solutions of different refractive indices. Figure 5(f) shows the line profile of the fringe pattern along the dashed white line shown in figures 5(a) to (d).

Figure 5 shows that as the refractive index of the solution inside the experimental chamber increases, the shift of the imaged fringe pattern also increases, compared to the imaged reference fringe pattern recorded after filling the experimental chamber with distilled deionized water. Supplementary video file Video V1 shows the change in the recorded line pattern as the refractive index inside the experimental chamber is increased, along with the line profile of the recorded pattern. The fringe patterns are then numerically processed using the Fourier fringe analysis algorithm to extract phase information, which was then used to quantify the refractive index of the solution.

4. Processing of the fringe pattern and feature extraction

The recorded image pattern (sinusoidal line pattern) is used to extract information regarding the refractive index of the solution inside the test chamber using Fourier fringe analysis technique, which is a powerful tool used to analyze patterns in interferometry and optical metrology [33, 35, 50]. By applying the Fourier transform to recorded fringe images, the method extracts gradient phase information from the intensity variations of the recorded fringe pattern, providing high-precision measurements of phase distributions [50]. Fourier spectra of all the recorded images were computed to extract phase (a flowchart of the process is shown in figure 2) and were filtered using a rectangular mask centred at the sideband. The filtered spectrum was then inverse Fourier transformed to yield the complex array $C(x, y)$. The whole process can be expressed as [50]

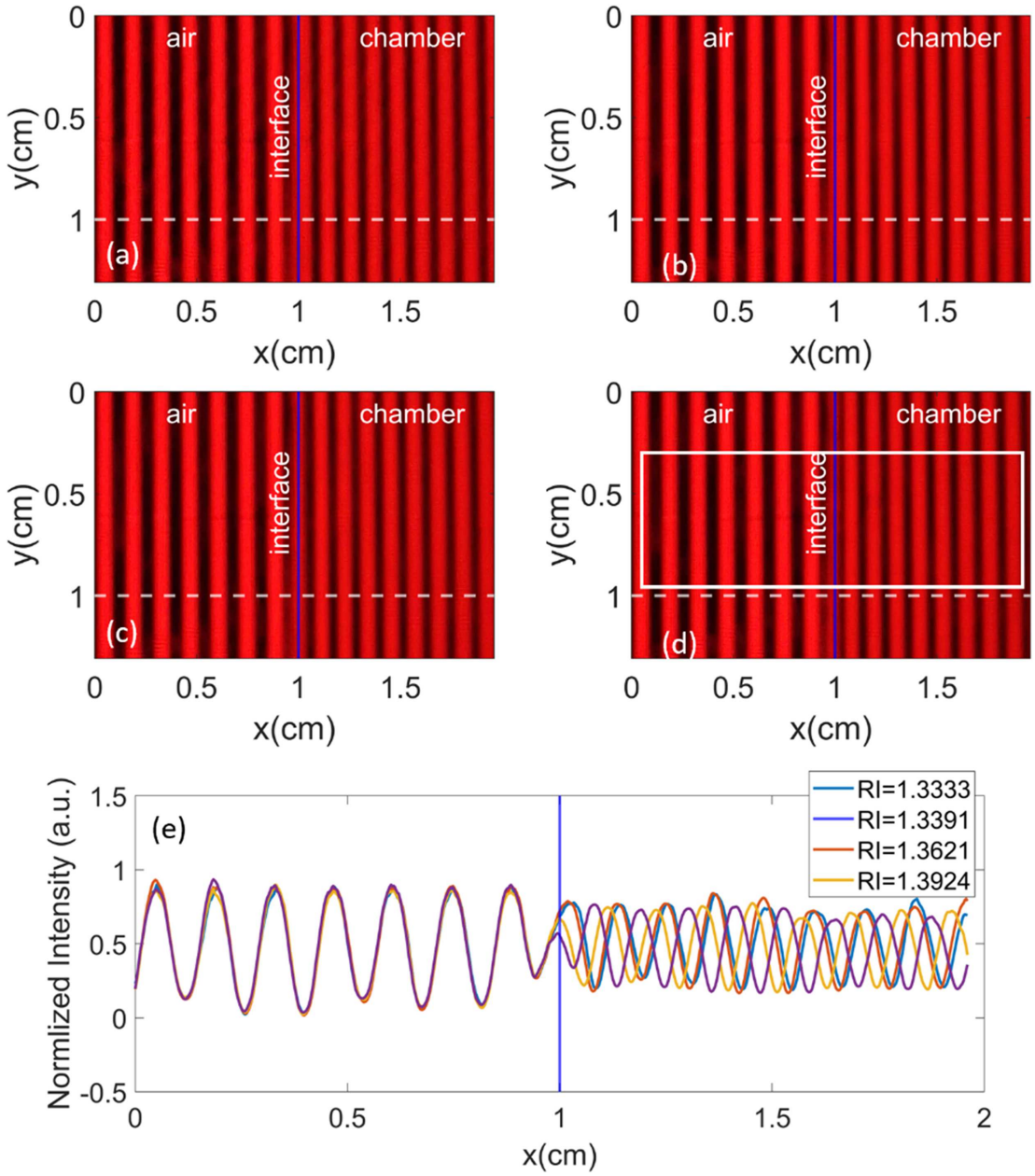

Figure 5. Recorded fringe patterns for solutions of different refractive (a) RI = 1.3333 (reference solution); (b) RI = 1.3391; (c) RI = 1.3621; (d) RI = 1.3924. (e) Profile of the recorded intensity pattern along the dashed line shown in figures 5(a) to (d).

$$C(x, y) = \mathcal{J}^{-1}[\overline{\mathcal{J}\{I(x, y)\}}] \tag{1}$$

Where $\mathcal{J}$ and $\mathcal{J}^{-1}$ represent the Fourier transform and inverse Fourier transform, respectively. In equation (1), $\mathcal{J}\{\overline{I(x, y)}\}$ represents the filtering of the Fourier spectrum of the recorded intensity pattern $I(x, y)$ for a particular test solution. The gradient phase is extracted from C using

$$\phi(x, y) = \tan^{-1}\left[\frac{\mathrm{Im}\{C(x, y)\}}{\mathrm{Re}\{C(x, y)\}}\right] \tag{2}$$

'Re' and 'Im' represent the real and imaginary parts, respectively. The gradient phase (ϕ_W) for the reference solution (DI water) was first extracted. The gradient phase distribution (ϕ_S) of the test solutions of varying refractive indices were then extracted. The gradient phase difference, $\Delta\phi = \phi_S - \phi_W$, was then computed. Figure 6 shows the computed gradient phase difference for solutions of different refractive indices. This figure indicates that as the refractive index of the solution inside the test chamber increases, the phase difference also increases.

This gradient phase difference was converted to phase difference by numerical integration along the direction of intensity change of the projected pattern (horizontal or x-direction in the present case). The computed

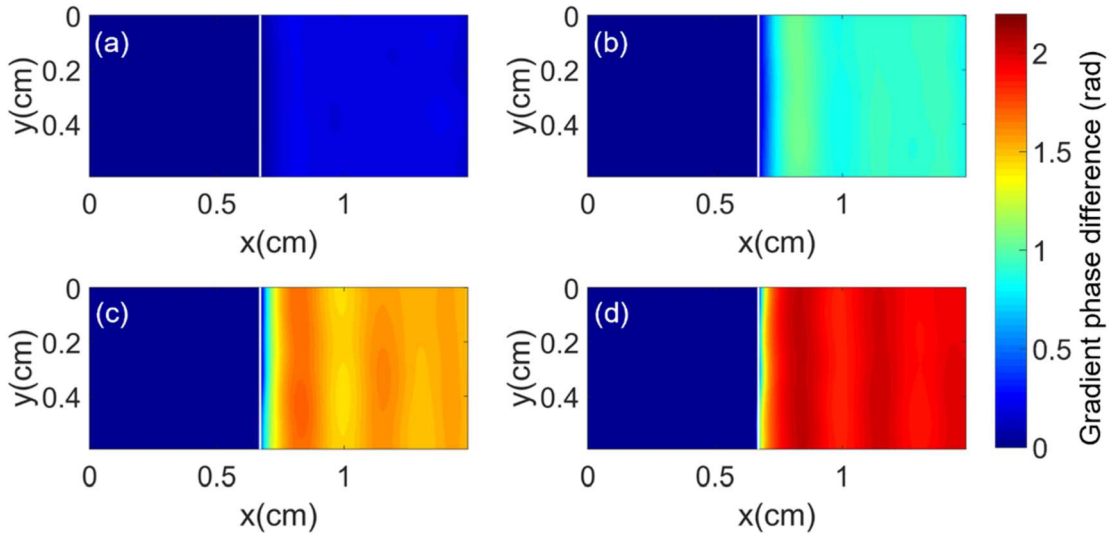

Figure 6. Computed gradient phase differences for solutions of different refractive indices. (a) RI = 1.3391; (b) RI = 1.3621; (c) RI = 1.3789; (d) RI = 1.3924. In all the cases, the reference solution was DI water (RI = 1.3333).

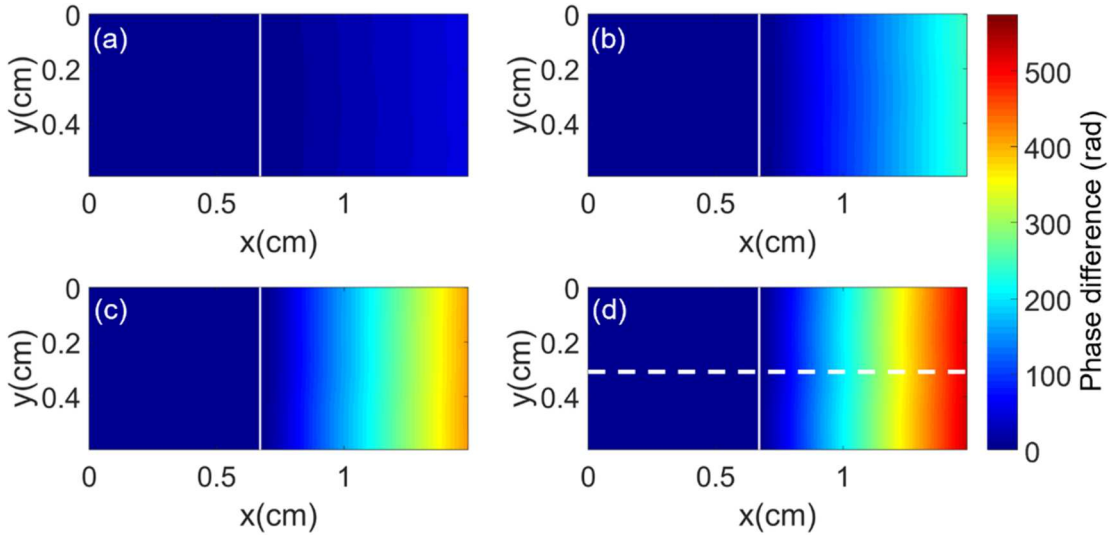

Figure 7. Computed phase differences for solutions of different refractive indices obtained after numerical integration of the gradient phase differences shown in figure 6. (a) RI = 1.3391; (b) RI = 1.3621; (c) RI = 1.3789; (d) RI = 1.3924. The reference solution in all cases was DI water (RI = 1.3333).

phase distribution is proportional to the fringe density p, the distance of the fringe pattern from the experimental chamber (d), and the optical path length difference [55]. The computed phase difference for solutions of different refractive indices is shown in figure 7.

Figure 8 shows the profile of the phase maps along the dashed white line shown in figure 7(d). Supplementary video file Video V2 shows the change in the computed phase difference profile as the refractive index of the solution inside the experimental chamber is increased, along with the line profile. Similarly, supplementary Video V3 is the three-dimensional rendering of the computed phase difference profile with an increase in refractive index.

Figures 7 and 8 indicate that the phase difference profile of the projected line pattern carries information regarding the refractive index of the solution inside the test chamber. Sample features based on the computed phase information were extracted. From figures 7 and 8, the most noticeable feature that could be used is the phase volume which is the sum of the computed phase values inside the chamber. Other extracted features are the mean of (i) the sum of phase profile along each row (direction of the optical thickness variation), (ii) maximum phase difference along each row, (iii) slope of the best fit to the phase profile along each row, (iv) intercept of the best fit to the phase profile along each row and (v) variance of phase profile along each row.

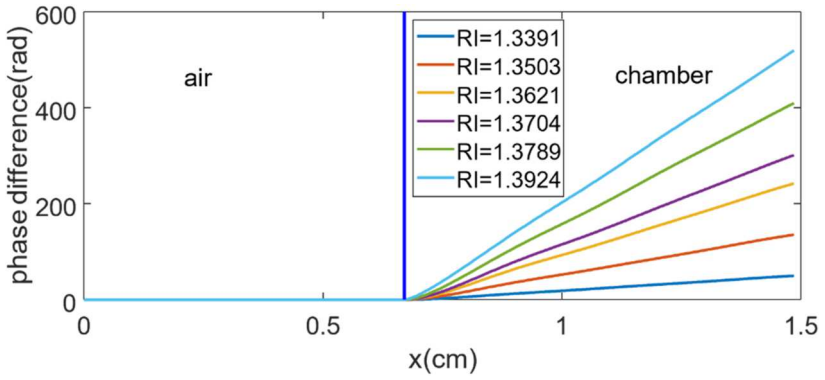

Figure 8. Phase profile along the dashed line shown in figure 7(d) for solutions of different concentrations.

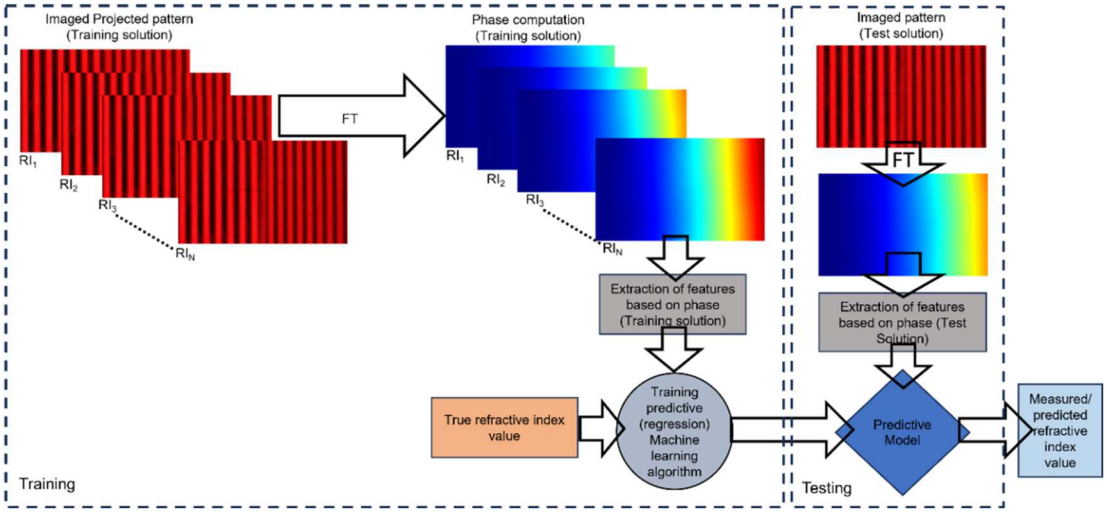

Figure 9. Numerical processing of the recorded pattern, phase feature extraction, training of regression algorithm, and testing of the trained predictive model for measurement of refractive index of transparent solutions.

5. Results and discussions

The described method predicts the refractive index values of liquid solutions using the extracted phase features from the phase deflectometric refractometer. For the prediction extracted features were used to train regression machine learning algorithms, leading to a predictive model [42, 43] as shown in figure 9, which was then used to predict refractive indices of unseen test solutions.

The extracted features had different magnitudes; hence, they were normalized (scaled) before the training step to ensure that features with higher magnitudes did not dominate the model [43]. The normalized data was used to build 30 training and test data pairs. For each pair, features corresponding to 11 randomly selected refractive index values (each with ten measurements, totalling 110 samples) were used for training, while the features of the remaining five refractive index values (each with ten measurements with a total of 50 samples), unseen during the training process, were reserved for testing. This type of splitting ensured that the algorithms were trained on different portions of the whole dataset and tested on unseen data, reducing overfitting and improving the prediciton accuracy of the resulting model. Various regression algorithms were trained on each pair of training and testing datasets to quantify the measurement errors of the generated predictive model [48, 49]. Multiple training and test sets also ensured that the entire refractive index range was used during the training and testing stages. The measurement errors were averaged across all training and test dataset pairs, providing a better evaluation of the measurement accuracy of the model and ensuring that the results were not biased by any particular split [57].

In developing a predictive model for refractive index estimation from the extracted phase features, it is advantageous to evaluate multiple predictive algorithms (techniques) to identify the most effective one. We trained and evaluated regression algorithms such as (i) Multiple Linear Regression (MLR), which identifies the

Table 1. Performance evaluation of various models (Training).

Model	RMSE	MAE	R^2
Multiple linear regression (MLR)	0.00074	0.00070	0.9979
Polynomial linear regression (PLR)	0.00071	0.00061	0.9982
Polynomial ridge regression (PRR)	0.00042	0.00036	0.9993
Decision tree regression (DTR)	0.00026	0.00011	0.9996
Random forest regression (RFR)	0.00023	0.00002	0.9997

Table 2. Performance evaluation of various models (Testing).

Model	RMSE	MAE	R^2
Multiple linear regression (MLR)	0.00091	0.00080	0.9948
Polynomial linear regression (PLR)	0.00091	0.00084	0.9945
Polynomial ridge regression (PRR)	0.00068	0.00062	0.9969
Decision tree regression (DTR)	0.00375	0.00367	0.9338
Random forest regression (RFR)	0.00458	0.00443	0.8954

linear relationships between phase features and the RI values and act as the base model [57], (ii) Support Vector Regression (SVR), which identifies non-linear relationships between the features and the RI values through kernels approach [58], (iii) Decision Tree Regression (DTR) and Random Forest Regression (RFR), that use tree based structures to model non-linear relationships and interactions among various phase features [57], (iv) Polynomial Linear Regression (PLR), which uses polynomial features (extracted phase features and their higher degrees) to identify non-linear relationships among them, with the model parameters kept linear, allowing the modeling of complex data patterns and (v) Polynomial Ridge Regression (PRR), which incorporates L2 regularization in PLR, thus preventing overfitting [58]. This evaluation ensures the selected model is efficient and robust, acting as a reliable source for RI predictions. The scikit-learn library in Python was used to train these above mentioned regression algorithms to generate model for prediction of RI [43, 59, 60]. The performance of these models was evaluated using Root Mean Square Error (RMSE), (Mean Absolute Error (MAE), and R^2 scores [43, 48, 49]. RMSE provides the average magnitude of the prediction errors (error sensitivity), where larger errors are penalized more, making it helpful in identifying significant deviations from real RI (ground truth) values. On the contrary, MAE provides the average of the absolute errors (average prediction error), which does not overemphasize the outliers (large deviations). The R^2 score measures how well the predicted RI values fit the actual RI values, quantifying the proportion of variance in the RI the model can explain.

While training the regression algorithms to generate the predictive models, five-fold cross-validation was used to assess the performance of the trained model. Cross-validation helps detect overfitting of the training data. Table 1 shows the performance indicators of different models while training. The model based on support vector regression was omitted since the R^2 score obtained during training was negative, suggesting an overfitting or the model is poorly suited to the data and does not capture the relationship between the features and the refractive to be predicted [43].

The model was then used to predict refractive indices using features from unseen data (test data, which was held out during the training and validation process) to evaluate the performance of the model in a completely new situation. This ensures a realistic estimate of how the model will perform when refractive index of unknown solutions is to be measured and that the performance metrics are not influenced by data used in training and validation stage, providing an accurate measure of the generalization capability of the model [57]. Table 2 shows the performance indicators of different trained models with unseen test data. In tables 1 and 2, PLR used a second-degree polynomial expansion, while PRR used a fourth-degree polynomial expansion of the extracted features.

Even though the RFR model provided the best RMSE, MAE, and R^2 values during the training and validation stage, it performed poorly in the testing stage, indicating that the model is unsuitable for RI prediction of unknown liquids. However, the performance metrics of the PRR model remained the same during the training and test stages. It provided the best RMSE, MAE, and R^2 values during the test stage and was selected to estimate refractive index values of unknown solutions.

Figure 10(a) shows the predicted refractive index during the training and cross-validation stage of the polynomial regression algorithm. The error bar represents the average RMSE (average deviation between predicted and true RI values or measure of average prediction error) for each refractive index computed from all the

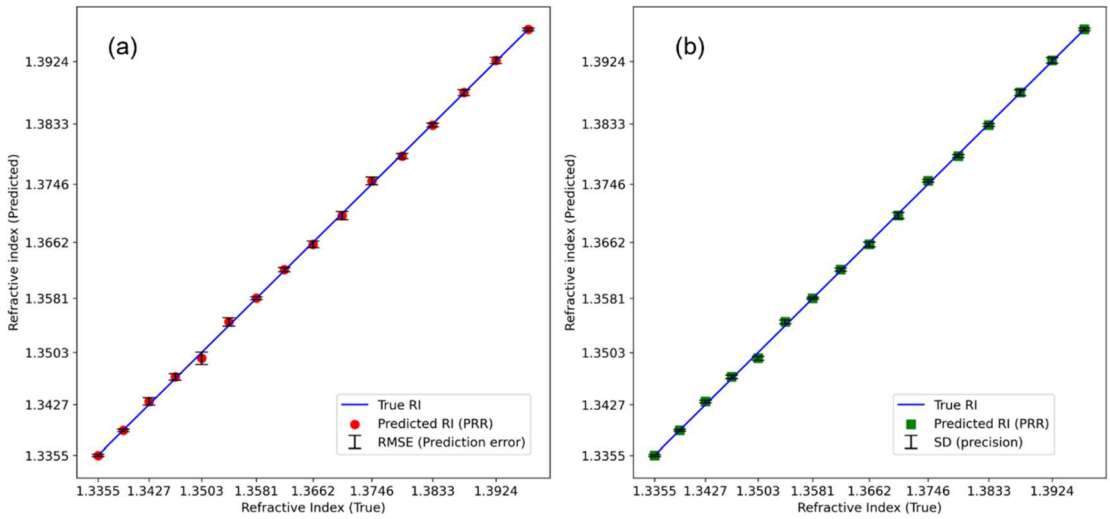

Figure 10. Performance of Polynomial Ridge Regression model in predicting RI values during training stage. (a) Prediction error; (b) Precision. The predicted refractive index is an average over the entire 30 training data sets. The average RMSE considering all training data sets was 0.00042. The average SD considering all training data sets was 0.00025.

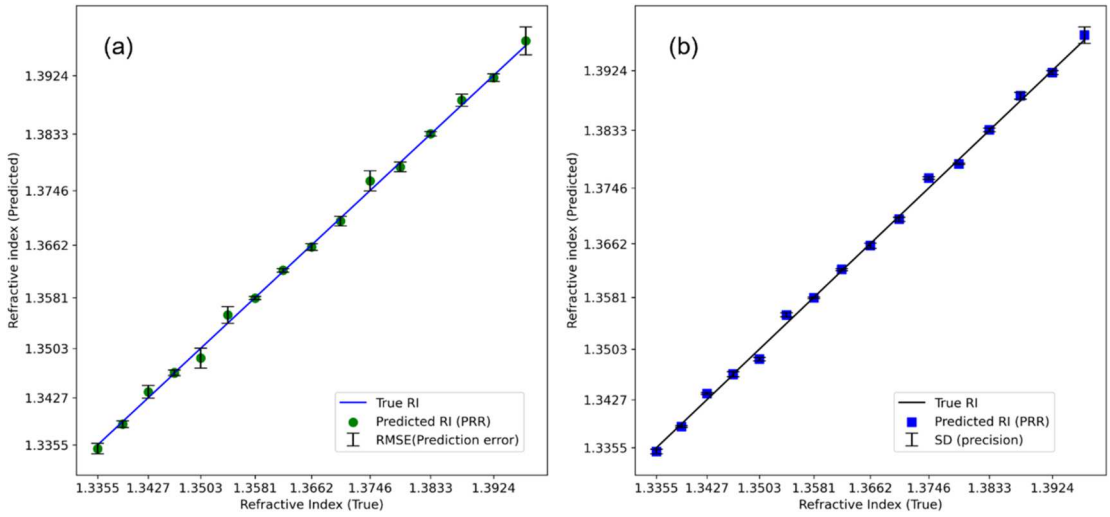

Figure 11. Performance of the trained Polynomial Ridge Regression model on unseen test data. (a) Prediction error; (b) Precision. For each RI, the value represents an average across 30 sets of test data (each set contains 10 measurements of 5 RI values). The average RMSE for test data was 0.00068, and average SD was 0.00026.

training data sets. Figure 10(b) shows the average of the standard deviation (SD), computed for each RI from multiple training data sets, which measures the precision of the predictions, reflecting the consistency of repeated measurements, with a lower SD indicating that the measurements are closely clustered around the predicted mean. The average of SD for considering all refractive indices was 0.00025. The average of MAE during the training stage, considering all RIs, was 0.00036 (table 1).

These metrics were also used to evaluate the model during testing phase figures 11(a) and (b) shows the RMSE and SD, respectively, when unseen test data was used to predict RI values using the trained PLR model. The obtained RMSE was 0.00068 with a SD of 0.00026 and MAE of 0.00062. Table 2 shows the values of different performance evaluation metrics during testing.

Ensemble methods such as gradient boosting, voting regression and stacking were also evaluated to identify if the accuracy and precision may be improved [58]. However, the performance of the models using these approaches was inferior to that of PRR. The performance metrics and evaluation of different regression schemes demonstrate that the proposed method, coupling phase deflectometry with a trained Polynomial Ridge Regression model, provides accurate refractive index measurement with high precision, with RMSE highlighting the general prediction accuracy, SD indicating precision, and MAE providing a more

Table 3. Predicted refractive indices from test data using features extracted from phase measuring deflectometry and PRR model.

True RI	Predicted RI	RMSE	MAE	SD
1.3355	1.3349	0.00080	0.00076	0.00034
1.3391	1.3387	0.00053	0.00052	0.00013
1.3427	1.3437	0.00098	0.00096	0.00012
1.3465	1.3465	0.00040	0.00034	0.00032
1.3503	1.3488	0.00155	0.00152	0.00025
1.3542	1.3555	0.00129	0.00125	0.00030
1.3581	1.3580	0.00024	0.00022	0.00012
1.3621	1.3623	0.00028	0.00024	0.00015
1.3662	1.3659	0.00051	0.00040	0.00040
1.3704	1.3699	0.00073	0.00065	0.00032
1.3746	1.3761	0.00154	0.00152	0.00020
1.3789	1.3783	0.00077	0.00076	0.00011
1.3833	1.3834	0.00035	0.00031	0.00026
1.3878	1.3886	0.00093	0.00079	0.00051
1.3924	1.3921	0.00060	0.00052	0.00031
1.3970	1.3977	0.00216	0.00188	0.00124

straightforward measure of prediction accuracy. Table 3 shows the predicted refractive indices for different sugar solutions along with true values and other measurement parameters.

While the present proof-of-concept study utilized a dataset of 160 samples spanning a broad range of refractive indices and concentrations representative of real-world liquids, this number was sufficient to train and evaluate the machine learning models with consistent performance across multiple cross-validation splits. The reported prediction accuracy (RMSE $= 8.5375 \times 10^{-4}$, MAE $= 7.9 \times 10^{-4}$) and low standard deviation of predicted values reflect good model generalizability and stability. The number of samples required to train a reliable regression model depends on the model's complexity and the number of input features. In this case, six phase-derived features and classical regression algorithms were employed, for which a common guideline suggests 10–30 times as many samples as features [61, 62]. The current dataset meets this criterion. Nevertheless, we are actively collecting additional measurements, including from different liquids, to further improve robustness and reliability. Since the central objective of this work was to establish the feasibility of PMD in transmission mode for refractive index measurement, detailed optimizations of optical geometry and the ML model—including dataset size variation—are planned for future studies.

6. Conclusions

The presented work was an effort to employ phase measuring deflectometry (PMD) for the development of a compact, portable, affordable, and simple refractometer for transparent liquids. The proposed technique used the concept of bending of light due to a change in the refractive index. A fringe pattern displayed on a smartphone screen, was imaged by a smartphone camera after passing through a hollow glass prism filled with liquids whose refractive index is to be determined. Liquids of different refractive indices induce different amounts of fringe shifts, which can be quantified in terms of change in phase. This phase difference was computed by comparing the phase associated with distilled water and the phase associated with sucrose solution using Fourier fringe analysis technique. The refractometer measures RI by extracting features based on the computed phase difference profile. These features are then used to train a regression machine learning algorithm to predict the RI values of unknown liquids. The best performance for predicting refractive index using phase features has been achieved with Polynomial Ridge Regression, yielding the lowest RMSE of 0.00067, MAE of 0.00062, and a standard deviation of 0.00026 (figure 11 and tables 2 and 3) across multiple unseen test datasets. Attempts to improve the model by stacking resulted in worse RMSE values.

Although the proposed technique requires a calibration, it offers several advantages. The use of smartphone screen for displaying fringe patterns allows for the ease of changing the fringe density, and its orientation which provides flexibility in changing the sensitivity and range of the RI measurement. Unlike digital holography and other interferometry-based techniques, the proposed technique does not require meeting stringent experimental conditions such as a separate light source, vibration isolation, and sufficient coherence length. The design and principle of the developed refractometer allow the system to be robust. In any measurement system, calibration refers to associating measured signals with known physical quantities, typically using standard reference conditions. In our setup, calibration maps the extracted phase change to known refractive indices

using distilled water as a reference. As such, minor realignments of optical components generally result in low-order phase offsets or scaling, which the machine learning model can partially accommodate.

To validate this, we initially calibrated the system with sugar solutions and observed a linear relationship between solution concentration and phase shift. This enables simplified recalibration: verifying a few known concentrations suffices to confirm alignment, avoiding full retraining. A brief recalibration is recommended if significant geometric changes are made to the optical geometry. This inherent tolerance enhances the system's robustness in real-world use.

While the current study focused on evaluating the system under ambient indoor lighting and standard laboratory conditions, the experiments were deliberately conducted without vibration isolation or specialized optics to reflect realistic use scenarios. The system demonstrated stable phase recovery and accurate RI prediction across 160 samples, supporting its robustness. Nonetheless, we acknowledge that further validation under more complex conditions—such as inhomogeneous, turbid, or multiphase liquids—will be important for expanding its applicability. These efforts are underway and will include testing under varying environmental factors and with broader fluid types to evaluate generalizability and limitations. This will form the basis of future work.

This is a proof-of-concept work for establishing PMD as a suitable technique for refractive index measurement of transparent liquid. The sensitivity and range of the proposed system can be further studied using fringe patterns of different orientations and densities and by using various fringe analysis approaches. Moreover, owing to its low-complexity design, the proposed technique can be converted into a hand-held portable device. In the proof-of-concept experiments, the basic ideas were to use simple regression algorithms to predict refractive index values. However, more advanced approach like Bayesian Optimization could be applied to tune hyperparameters of models like Polynomial Ridge Regression or Random Forest Regression (RFR), which is presently being investigated. Neural network-based regressors may also yield improvements and will be investigated in the future with more refractive index data. The shape of the experimental cell may also affect the prediction accuracy as for example a cell with a curved surface may provide more phase features compared to the prism used in the present case, which may be beneficial. Presently, work is progressing in this direction.

Declaration of competing interest

The authors declare that they have no known competing financial interests or personal relationships that could have appeared to influence the work reported in this paper.

Acknowledgments

Shivam Sharma would like to acknowledge UGC for SRF. Vismay Trivedi would like to acknowledge SERB for N-PDF. The work was supported by research grants from SERB (EMR/2017/002724), DAE-BRNS (2013/34/11/BRNS/504), DST-FIST, and DST-PURSE. SU and AA thank ICTP, Trieste, Italy, for the STEP and the TRIL fellowships, respectively.

Conflicts of interest

There are no conflicts to declare.

Data availability statement

The data includes raw images and processed phase maps specific to our experimental setup. Due to their size and context-dependent nature, they are best shared upon request to ensure proper interpretation and responsible use. The data that support the findings of this study are available upon reasonable request from the authors.

Author contributions

Shivam Sharma
Formal analysis (equal), Investigation (equal), Software (equal), Validation (equal), Writing – original draft (equal), Methodology (equal)

Vismay Trivedi 0009-0002-7792-7990
Formal analysis (equal), Investigation (equal), Methodology (equal), Project administration (equal), Validation (equal), Writing – original draft (equal), Writing – review & editing (equal)

Subhash Utadiya
Formal analysis (equal), Investigation (equal), Methodology (equal)

Gyanendra Sheoran 0000-0002-9631-9707
Validation (equal), Writing – review & editing (equal)

Arun Anand 0000-0003-3210-8676
Conceptualization (equal), Formal analysis (equal), Funding acquisition (equal), Project administration (equal), Software (equal), Supervision (equal), Writing – original draft (equal), Writing – review & editing (equal)

References

[1] Hecht E 2002 *Optics* (Addison-Wesley)
[2] Rivera-Ortega U, Hernández-Gómez C R, Vega-Torres G and Lopez-Medina M E 2018 Simple apparatus to calculate the refractive index of liquids based on Snell's law *Measurement* **134** 658–61
[3] Duprat F, Ploix J-L, Aubry J-M and Gaudin T 2023 Fast and accurate prediction of refractive index of organic liquids with graph machines *Molecules* **28** 6805
[4] Jaywant S A, Singh H and Arif K M 2022 Sensors and instruments for brix measurement: a review *Sensors* **22** 1–20
[5] Khan A S *et al* 2018 Preharvest Sprays Affecting Shelf Life and Storage Potential of Fruits *Preharvest Modulation of Postharvest Fruit and Vegetable Quality* 1st end, ed M W Siddiqui (Elsevier) 9 209–55
[6] Wilson D 2021 Chemical sensors for farm-to-table monitoring of fruit quality *Sensors* **21**
[7] Vilitis O, Shipkovs P and Merkulov D 2009 Determining the refractive index of liquids using a cylindrical cuvette *Meas. Sci. Technol.* **20** 117001
[8] Wan J, Lu Y, Li X, Zhang Z, Yang J, Jiang G and Hu F 2017 Liquid prism based refractometer *Journal of Optics* **19** 055705
[9] Yunus W M and Rahman A B 1988 Refractive index of solutions at high concentrations *Appl. Opt.* **27** 3341–3
[10] Liu P Y *et al* 2016 Cell refractive index for cell biology and disease diagnosis: past, present and future *Lab Chip* **16** 634–44
[11] Chetia D, Basumatary T, Singh H K and Bezboruah T 2016 Low-cost refractometer with longitudinally displaced optical fibers *IEEE Sens. J.* **16** 5950–7
[12] Jin Y L, Chen J Y, Xu L and Wang P N 2006 Refractive index measurement for biomaterial samples by total internal reflection *Phys. Med. Biol.* **51** N371–9
[13] Trivedi V, Joglekar M, Mahajan S, Patel N, Chhaniwal V, Javidi B and Anand A 2019 Digital holographic imaging of refractive index distributions for defect detection *Opt. Laser Technol.* **111** 439–46
[14] Patil J J, Patil Y H and Ghosh A 2020 Comprehensive and analytical review on optical fiber refractive index sensor *Proc. of the 4th Int. Conf. on Trends in Electronics and Informatics, ICOEI 2020*
[15] Koohyar F 2013 Refractive index and its applications *Journal of Thermodynamics & Catalysis* **4** 1
[16] Mohan S, Kato E, Drennen J K and Anderson C A 2019 Refractive index measurement of pharmaceutical solids: a review of measurement methods and pharmaceutical applications *J. Pharm. Sci.* **108** 3478–95
[17] Putnam D F 1971 *Composition and Concentrative Properties of Human Urine Dac-61125-f* NASA 109 Composition and concentrative properties of human urine
[18] Grange B W, Stevenson W H and Viskanta R 1976 Refractive index of liquid solutions at low temperatures: an accurate measurement *Appl. Opt.* **15** 858
[19] Idris N, Maswati and Yusibani E 2018 Influence of the apex angle of a hollow prism made from an ordinary commercial glass plate as a simple refractometer to the accuracy of the refractive index measurement of the edible oil *IOP Conf. Ser.: Mater. Sci. Eng.* **352** 012045
[20] Kruger O and Chetty N 2021 Development of a permanent vacuum hollow prism air refractometer for use in dimensional metrology *Sci Rep.* **11** 1–8
[21] An Y K 2017 Simple method to measure the refractive index of liquid with graduated cylinder and beaker *Rev. Sci. Instrum.* **88** 125105
[22] Chiu M-H, Hsu S-N and Yang H 2004 D-type fiber optic sensor used as a refractometer based on total-internal reflection heterodyne interferometry *Sensors Actuators* B **101** 322–7
[23] Banerjee A, Mukherjee S, Verma R K, Jana B, Khan T K, Chakroborty M, Das R, Biswas S, Saxena A and Singh V 2007 Fiber optic sensing of liquid refractive index *Sensors Actuators* B **123** 594–605
[24] Singh H K, Chamuah N, Sarkar D and Bezboruah T 2014 Non-intrusive technique for measuring refractive index of clear and transparent liquids *IEEE Sens. J.* **14** 313–4
[25] Tou Z Q, Chan C C, Wong W C and Chen L H 2013 Fiber optic refractometer based on cladding excitation of localized surface plasmon resonance *IEEE Photonics Technol. Lett.* **25** 556–9
[26] Jha R, Villatoro J, Badenes G and Pruneri V 2009 Refractometry based on a photonic crystal fiber interferometer *Opt. Lett.* **34** 617
[27] Tran V, Sahoo S K, Wang D and Dang C 2020 Utilizing multiple scattering effect for highly sensitive optical refractive index sensing *Sensors Actuators* A **301** 111776
[28] Facchin M, Bruce G D and Dholakia K 2022 Correction to 'Measurement of variations in gas refractive index with 10 –9 resolution using laser speckle *ACS Photonics* **9** 830–836
[29] Trivedi V, Mahajan S, Joglekar M, Chhaniwal V, Zalevsky Z, Javidi B and Anand A 2019 3D printed hand-held refractometer based on laser speckle correlation *Opt. Lasers Eng.* **118** 7–13
[30] Utadiya S, Trivedi V, Sheoran G, Srivastava A, Claus D, Cabrera H and Anand A 2023 Digital holographic imaging of thermal signatures and its use in inhomogeneity identification *Opt. Lasers Eng.* **160** 107227

[31] Utadiya S, Trivedi V, Bhanderi K, Joglekar M, Limberkar C, Patel K, Sheoran G, Cabrera H, Javidi B and Anand A 2023 Thickness and surface profiling of optically transparent and reflecting samples using lens-less self-referencing digital holographic microscopy *Applied Surface Science Advances* **18** 100484
[32] Utadiya S, Trivedi V, Srivastava A, Cabrera H, Crespo M L, Sheoran G and Anand A 2024 Optical thickness measurement of occluded samples by lens-less Fourier transform digital holography, thermal loading, and machine learning *Appl. Opt.* **63** B16
[33] Trivedi V, Joglekar M, Utadiya S, Chhiller N, Sharma S, Sheoran G and Anand A 2023 Shape measurement of phase objects using fringe projection technique *Optical Measurement Systems for Industrial Inspection XIII* ed P Lehmann *et al* (SPIE) 104
[34] Chhaniwal V K, Narayanamurthy C S and Anand A 2014 Imaging of mass transfer process using artificial fringe deflection *Opt. Eng.* **53** 074106
[35] Trivedi V, Joglekar M, Mahajan S, Chhaniwal V, Javidi B and Anand A 2019 Portable device based on beam deflection for refractive index mapping and diffusion coefficient measurement *Opt. Eng.* **58** 1
[36] Guo H, Zhou H and Banerjee P P 2022 Use of structured light in 3D reconstruction of transparent objects *Appl. Opt.* **61** B314
[37] Xu Y, Gao F and Jiang X 2020 A brief review of the technological advancements of phase measuring deflectometry *PhotoniX* **1** 14
[38] Huang P S and Zhang S 2006 Fast three-step phase-shifting algorithm *Appl. Opt.* **45** 5086
[39] Kemao Q 2007 Two-dimensional windowed Fourier transform for fringe pattern analysis: principles, applications and implementations *Opt. Lasers Eng.* **45** 304–17
[40] Sharma S, Trivedi V, Mahajan S, Sheoran G, Javidi B and Anand A 2025 Phase measuring deflectometry based microscopy for shape visualization and thickness quantification *Opt. Laser Technol.* **192** 113524
[41] Trivedi R, Sharma S, Trivedi V, Sharma R, Groves R M, Sheoran G and Anand A 2025 Heat flow visualization and thermal anomaly detection using phase measuring deflectometry *Optical Measurement Systems for Industrial Inspection XIV* ed P Lehmann *et al* (SPIE) 101
[42] James G, Witten D, Hastie T and Tibshirani R 2000 *An introduction to Statistical Learning* (*Springer Texts in Statistics*) 7 2nd edn (Springer) 1–450
[43] Müller A and Guido S 2018 *Introduction to machine learning with python: a guide for data scientists* 1st edn (O'Reilly Media)
[44] Mohd Noor M Y, Azizan A, Saimon S M, Azmi A I, Iqbal F, Abdullah A S, Zhang J and Shapiai M I 2024 Decision tree regression supervised machine learning assisted large dynamic range refractive index detection using MMI coreless multimode fiber sensor *IEEE Sens. J.* **24** 12403–40
[45] Martinez-Manuel R, Valentin-Coronado L M, Esquivel-Hernandez J, Monga K J J and Larochelle S 2022 Machine learning implementation for unambiguous refractive index measurement using a self-referenced fiber refractometer *IEEE Sens. J.* **22** 14134–41
[46] Badloe T, Yang Y, Lee S, Jeon D, Youn J, Kim D S and Rho J 2024 Artificial intelligence-enhanced metasurfaces for instantaneous measurements of dispersive refractive index *Adv. Sci.* **11** 2403143
[47] Gu L, Gao H and Hu H 2023 Demonstration of a learning-empowered fiber specklegram sensor based on focused ion beam milling for refractive index sensing *Nanomaterials* **13** 768
[48] Vining G G 2011 *Statistical Methods for Engineers* (Cengage Learning)
[49] Doebelin E O 2004 *Measurement Systems: Application and Design* (McGraw-Hill)
[50] Born M, Wolf E, Bhatia A B, Clemmow P C, Gabor D, Stokes A R, Taylor A M, Wayman P A and Wilcock W L 1999 *Principles of Optics* (Cambridge University Press)
[51] Gorthi S S and Rastogi P 2010 Fringe projection techniques: Whither we are? *Opt. Lasers Eng.* **48** 133–40
[52] Zendejas-Hernández E, Trujillo-Schiaffino G, Anguiano-Morales M, Salas-Peimbert D P, Corral-Martínez L F and Tornero-Martínez N 2023 Spatial and temporal methods for fringe pattern analysis: a review *J. Opt.* **52** 888–99
[53] Takeda M and Mutoh K 1983 Fourier transform profilometry for the automatic measurement of 3D object shapes *Appl. Opt.* **22** 3977
[54] Huang L, Idir M, Zuo C and Asundi A 2018 Review of phase measuring deflectometry *Opt. Lasers Eng.* **107** 247–57
[55] Flores J L, Bravo-Medina B and Ferrari J A 2013 One-frame two-dimensional deflectometry for phase retrieval by addition of orthogonal fringe patterns *Appl. Opt.* **52** 6537
[56] Snyder C F and Hattenburg A T 1963 *Refractive Indices and Densities of Aqueous Solutions of Invert Sugar* NBS Monograph 64 U.S. Department of Commerce, National Bureau of Standards 1–6 Gaithersburg, MD
[57] Murphy K P 2012 *Machine Learning - A Probabilistic Perspective* (The MIT Press)
[58] Mark F 2019 *Machine Learning with Python for Everyone* (Pearson Education)
[59] Pedregosa F *et al* 2011 Scikit-learn: machine learning in Python *Journal of Machine Learning Research* **12** 2825–30
[60] Aurélien G 2019 *Hands-on Machine Learning with Scikit-Learn, Keras and TensorFlow: Concepts, Tools, and Techniques to Build Intelligent Systems* 2nd edn (O'Reilly Media)
[61] Silvey S and Liu J 2024 Sample size requirements for popular classification algorithms in tabular clinical data: empirical study *J Med Internet Res* **26** e60231
[62] Alwosheel A, van Cranenburgh S and Chorus C G 2018 Is your dataset big enough? Sample size requirements when using artificial neural networks for discrete choice analysis *Journal of Choice Modelling* **28** 167–82